Kinematic Creep in a Continuously Variable Transmission: Traction Drive Mechanics for Cobots
R. Brent Gillespie, Carl A. Moore, Michael Peshkin, and J. Edward Colgate
ASME J. Mechanical Design 124, 713 (2002)

Kinematic Creep in a Continuously Variable Transmission: Traction Drive Mechanics for Cobots

R. Brent Gillespie
Department of Mechanical Engineering,
University of Michigan,
Ann Arbor, MI 48109
e-mail: brentg@umich.edu

Carl A. Moore
Department of Mechanical Engineering,
Florida State University,
Tallahasee, FL 32310
email: camoore@eng.fsu.edu

Michael Peshkin

J. Edward Colgate

Department of Mechanical Engineering,
Northwestern University,
Evanston, Illinois 60208
e-mail: peshkin,colgate@nwu.edu

Two continuously variable transmissions are examined, one that relates a pair of linear speeds and another that relates a pair of angular speeds. These devices are elemental in the design of cobots, a new class of robot that creates virtual guiding surfaces to aid a human operator in assembly tasks. Both of these transmissions are traction drive mechanisms that rely on the support of either lateral or longitudinal forces across rolling contacts with spin. When a rolling contact between elastic bodies or even between rigid bodies in spin is called upon to transmit a tractive force, kinematic creep develops, expressing a departure from the intended rolling constraint. Creep in turn gives rise to nonideal properties in a cobot's virtual guiding surfaces. This paper develops simple models of the two transmissions by expressing the relative velocity field in the contact patch between rolling bodies in terms of creep and spin. Coulomb friction laws are applied in a quasi-static analysis to produce complete force-motion models. These models may be used to evaluate a cobot's ability to support forces against its virtual guiding surfaces. [DOI: 10.1115/1.1517560]

1 Introduction

In an ideal transmission, one would expect both the ratio of output to input shaft speeds and the ratio of input to output applied torques to take on the same value as the transmission ratio setting. Further, the value of the speed ratio would have no dependence on the torque transmitted through the transmission and the value of the torque ratio would have no dependence on the speed at which the transmission runs. An ideal transmission would also consume no power. Although behavior approaching the ideal can generally be expected of transmissions realized using gears, significant deviations from the ideal can be expected of transmissions realized using tractive rolling contacts. Some of the most promising continuously variable transmission (CVT) designs depend on tractive rolling. In traction drive CVTs, one can expect deviations of the speed ratio from the pre-set transmission ratio that grow steadily as the torque load increases and eventually give way to gross slip. These performance limitations are largely responsible for the low success rate of traction drive CVTs in demanding applications.

The behavior of a traction drive CVT, including deviation and eventual breakdown in its transmission laws, depends on the mechanics of contact at each internal rolling interface. A physically realizable rolling constraint is not impervious to the tangential forces (also called tractive forces or simply traction) transmitted across the contact between rolling surfaces. Traction induces elastic deformations and changes in the regions of sticking and slipping within the finite size contact patch, causing the rolling constraint to deviate from that dictated by the nominal wheel and rolling surface geometry.

In this paper, we investigate deviation of the speed ratio from the transmission ratio setting as a function of transmitted torque in a particular CVT design. Our CVT uses tractive rolling between two cylindrical wheels (known as drive rollers) and a rotating sphere. An additional pair of wheels (known as steering rollers) acts to orient the rotational axis of the sphere and thereby set the transmission ratio. A prototype CVT is shown in Fig. 1. The CVT design is further documented in [1] and [2].

To assess the effects of imperfectly held rolling constraints on the performance of our CVT, we look internal to the device: at each finite size contact patch between drive wheel and sphere. We construct a detailed kinematic model that includes rolling (sticking) and slipping regions within each contact patch. We define and apply nondimensionalized creep and spin parameters to the description of the relative velocity field in each contact patch and then find the resultant tractive forces by application of the Coulomb friction laws. Finally, a full kinetic model relates the nonideal transmission law for speed to the torque load.

1.1 CVTs for Cobots. Our interest in CVTs stems from their role in the design and construction of cobots. Cobots are a new class of robotic device, designed to carry out manipulation tasks in *cooperation* with a human. While the cobot and human simultaneously grasp an object to be manipulated, the human pro-

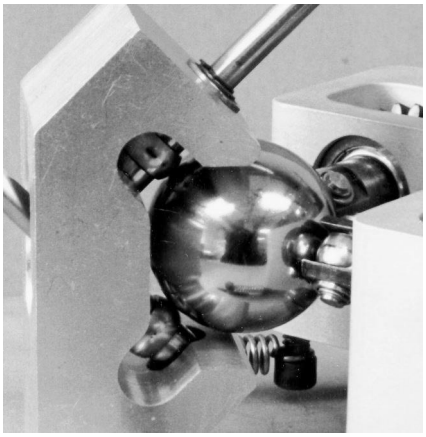

Fig. 1 Photograph of the prototype CVT. The drive rollers with axes in the vertical plane are visible on the left while the steering rollers with axes in the horizontal plane are visible on the right.

Contributed by the Mechanisms Committee for publication in the JOURNAL OF MECHANICAL DESIGN. Manuscript received September 1999. Associate Editor: C.W. Wampler II.

vides motive forces and the cobot directs motion using programmable motion constraints. Motion in only one instantaneously defined direction is allowed by the cobot. Using software control over the direction of the motion constraints, the cobot creates virtual fixtures within the shared workspace. The human can use these fixtures as guiding surfaces to develop superior manipulation strategies. To realize motion constraints at its end-effector, a cobot relies on a network of CVTs. The motion constraints are rendered programmable by active tuning of the CVT transmission ratios according to sensed human-applied force and sensed end-effector configuration.

There are two types of CVT used to construct cobots. The first is a simple steered wheel rolling on a planar surface. The steered wheel relates two linear speeds and supports forces acting in the direction of the wheel axel. The second type of CVT is the one treated in detail in this paper: the sphere-based CVT mentioned above. The sphere-based CVT relates two angular speeds and supports a certain ratio of input to output torques. Note that the wheel may be considered a *translational* CVT while the sphere-based CVT represents the more traditional application of the term CVT: as a *rotational* device.

Rolling contacts have been treated extensively in the literature. Models have been developed to describe the gradual breakdown and eventual failure of a rolling constraint under applied longitudinal or lateral loads. The tangential traction and twisting moment have been expressed as functions of relative motion in a planar contact patch for conditions of fully developed sliding in both analytic [3] and computational models [4]. Howe and Cutkosky have applied such models to problems in sliding manipulation control [5]. Certain models account for elasticity in the wheel or rolling surface and account for the effects of spin or cornering. Johnson [6] contains a particularly good review of rolling contact models.

Traction drive CVTs (as well as belt-drive CVTs) are being aggressively developed for application in automobiles, where they promise to increase fuel efficiency and driveability by eliminating gear shifting. Although these traction drive CVTs transmit tractive forces across rolling contacts like the CVT analyzed here, they also rely on the development of shear forces across a film of elastohydrodynamic oil that impinges between the rolling surfaces. The oil develops high viscosity under the high pressures in the rolling contact. This design has proven effective for the high torque transmission requirements of the automotive application. In contrast, the CVT analyzed in this paper uses dry friction between rolling bodies in direct contact. For a review of CVT designs for automotive applicaiton, see [7] and [8]. The CVT considered in this paper is very similar to the design developed for use in mobile robots described in [9] and the design developed for a nonholonomic manipulator described in [10]. A spherical rolling surface between a drive and driven wheel whose spin axis is rotated is common to all these designs. An analysis considering the mechanics of rolling contact in this CVT design has not been previously undertaken.

Our aim in this paper is to apply models of rolling contact to the CVT, to determine the manner in which traction-induced creep at each of the drive wheels expresses itself in deviations of the transmission law from the ideal. Our investigation is largely motivated by a suspected breakdown, for certain transmission ratio settings, of our CVT's ability to maintain its speed constraint while supporting a load. When the rotational axis of the sphere passes through the contact patch of one of the drive rollers (a condition which occurs for transmission ratio values of zero or infinity), the slip in that roller's contact patch is dominated by spin. In such case, one might intuitively expect that that drive roller is no longer capable of transmitting a longitudinal traction. A small torque load might then lead to loss of function (breakdown in the transmission law). To answer this question, we develop the simplest competent model of the CVT that may be used to relate nonideal performance characteristics to design parameters.

Prior to introducing the CVT, we discuss the steered wheel, which relates two linear speeds and force measure numbers rather than angular speeds and torque measure numbers. We introduce the ideal steered wheel and its function as a transmission in section 2. Section 3 introduces the CVT and presents its ideal kinematic and kinetic equations and establishes the analogy to the steered wheel. Section 4 introduces sideslip (lateral creep) in the steered wheel by referencing a simple model of an elastic Wheel. Section 5 presents a rigid body model of the CVT which features rigid drive rollers in tractive rolling with cornering. The nondimensionalized variables *creep* and *spin* are introduced and shown to be particularly advantageous descriptors of the kinematics of rolling since the tractive force may be simply expressed in terms of these variables. Finally, the full kinematic and kinetic equations are developed for the nonideal CVT. Deviations from the ideal are interpreted as a sideslip angle.

2 The Ideal Thin Wheel

We begin by developing the kinetics of a very simple system, the ideal thin wheel. This treatment will provide a point of departure for a discussion of the kinetics of the CVT. Figure 2 shows a thin wheel W of radius R in contact with a horizontal plane at point C. Mutually perpendicular unit vectors $\mathbf{n}_1$ and $\mathbf{n}_2$ are fixed in the plane as shown while $\mathbf{n}_3=\mathbf{n}_1\times\mathbf{n}_2$ defines the vertical. Let $\mathbf{b}_1$, $\mathbf{b}_2$, and $\mathbf{b}_3$ form a second right-handed set of orthogonal unit vectors, with $\mathbf{b}_2$ parallel to the lateral (axial) direction of W, $\mathbf{b}_1$ parallel to the longitudinal direction of W, and $\mathbf{b}_3$ parallel to the steering axis of W. The steering axis is maintained vertical (parallel to $\mathbf{n}_3$) by a support not shown. The angle γ subtended by $\mathbf{n}_1$ and $\mathbf{b}_1$ is called the steering angle; it is controlled by a motor.

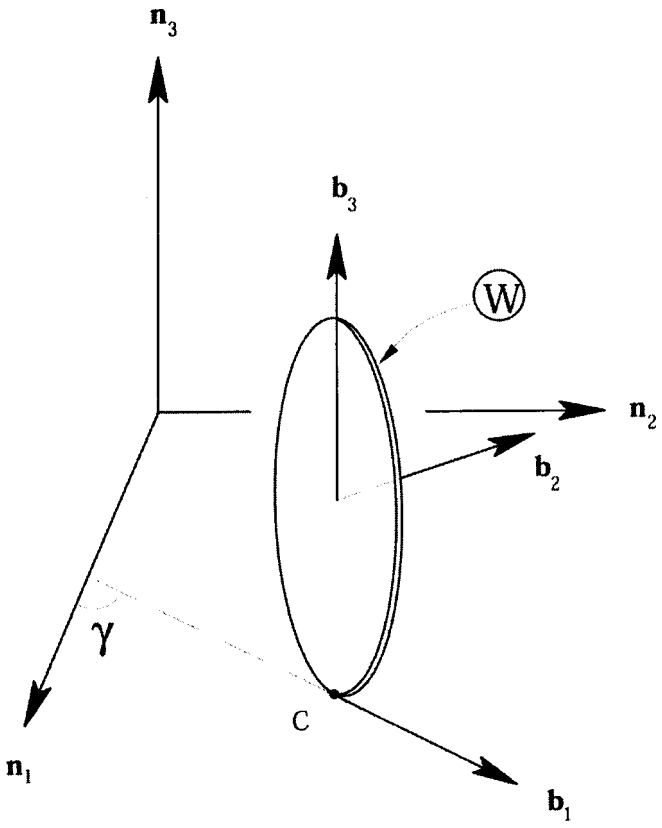

Fig. 2 Thin wheel with heading $\mathbf{b}_1$ and steering axis $\mathbf{b}_3$. The steering angle is γ.

Express the velocity of the contact point C in basis N as ${}^N\mathbf{v}^C = v_1\mathbf{n}_1 + v_2\mathbf{n}_2$, where the scalars v_1 and v_2 are called the N-measure numbers of ${}^N\mathbf{v}^C$. The ideal wheel allows motion of the contact point C in the longitudinal direction, yet prevents motion of C in the lateral direction: ${}^N\mathbf{v}^C \cdot \mathbf{b}_2 = 0$. This stipulation may be expressed in the N basis, where it reads:

$$\frac{v_2}{v_1} = \tan(\gamma). \tag{1}$$

Thus the wheel can be viewed as a continuously variable transmission, setting the ratio of two translational speeds.

2.1 Force Balance. Let a force $\mathbf{F}$ applied to the wheel through its axle be expressed in the N basis as $\mathbf{F} = f_1\mathbf{n}_1 + f_2\mathbf{n}_2$. The ideal wheel supports the lateral component of $\mathbf{F}$ with a friction force across the contact point C. Yet the wheel accelerates in response to any longitudinal component of $\mathbf{F}$. For steady motion, the longitudinal component of $\mathbf{F}$ must be zero, which reads in basis N:

$$\frac{f_1}{f_2} = -\tan(\gamma) \tag{2}$$

2.2 Coupling Space. To further elaborate on the function of the steered wheel as a continuously variable transmission, we introduce an abstract configuration space, which we label Σ and call *coupling space*. For the wheel, the axes of coupling space are associated with the linear displacements whose derivatives (speeds) are related by the transmission ratio. Thus the vectors spanning Σ-space, $\boldsymbol{\sigma}_1$ and $\boldsymbol{\sigma}_2$, are the same as $\mathbf{n}_1$ and $\mathbf{n}_2$, respectively.

We introduce a second basis U comprising unit vectors $\mathbf{u}_\parallel$ which defines the *allowed* direction and $\mathbf{u}_\perp$ which defines the *disallowed* direction. In the case of the wheel, $\mathbf{u}_\parallel$ is parallel to $\mathbf{b}_1$ and $\mathbf{u}_\perp$ is parallel to $\mathbf{b}_2$. The steered wheel allows motion in the $\mathbf{u}_\parallel$ direction yet resists motion in the $\mathbf{u}_\perp$ direction. Conversely, the wheel supports forces applied in the $\mathbf{u}_\perp$ direction, while steady motion requires that no force be applied in the $\mathbf{u}_\parallel$ direction. Thus we may state, regarding the U-measure numbers of the velocity of C and the force which may be supported across C in steady motion:

$$\begin{aligned} v_\perp &= 0 \\ f_\parallel &= 0. \end{aligned} \tag{3}$$

These statements, when rotated through the angle γ (re-expressed in the Σ basis) produce Eqs. (1) and (2).

In the case of the wheel, coupling space adds nothing new to the discussion. We introduce coupling space for the wheel in order to later draw analogies to the CVT (where Σ and U are nontrivially related to the bases describing the physical kinematics).

3 The Ideal Rotational CVT

Whereas the linear CVT (the steered wheel) employs one rolling contact, the rotational CVT employs four, making the kinematics of the rotational CVT significantly more complex. The construction of the rotational CVT involves a sphere of radius R in rolling contact with four cylindrical rollers, each of radius r. Figure 3 shows two schematic views of the CVT. Rollers $W1$ and $W2$, called the drive rollers, appear with the sphere S in Fig. 3(a). The drive rollers have fixed, co-planar axes. Rollers $R1$ and $R2$, called the steering rollers, appear with S in Fig. 3(b). The steering rollers rotate freely about axes which may be oriented by steering. A reference basis A, fixed in the base of the CVT, and comprising three orthogonal unit vectors $\mathbf{a}_i$ ($i = 1,2,3$) is shown in both views (a) and (b). A second base-fixed basis N (seen in Fig. 3(a)) is established by rotating basis A about $\mathbf{a}_2$ through $-45°$ while a third base-fixed basis B (seen in Fig. 3(b)) is established by rotating A about $\mathbf{a}_1$ through $+45°$. The axis of steering roller $R1$, shown parallel to $\mathbf{b}_2$, is oriented by rotation about $-\mathbf{b}_3$ through the steering angle ϕ. Similarly, the axis of steering roller $R2$, shown parallel to $\mathbf{b}_3$, is oriented by rotation about $\mathbf{b}_2$ through the same steering angle ϕ. The steering angle settings of rollers $R1$ and $R2$ are coupled through a set of bevel gears not shown.

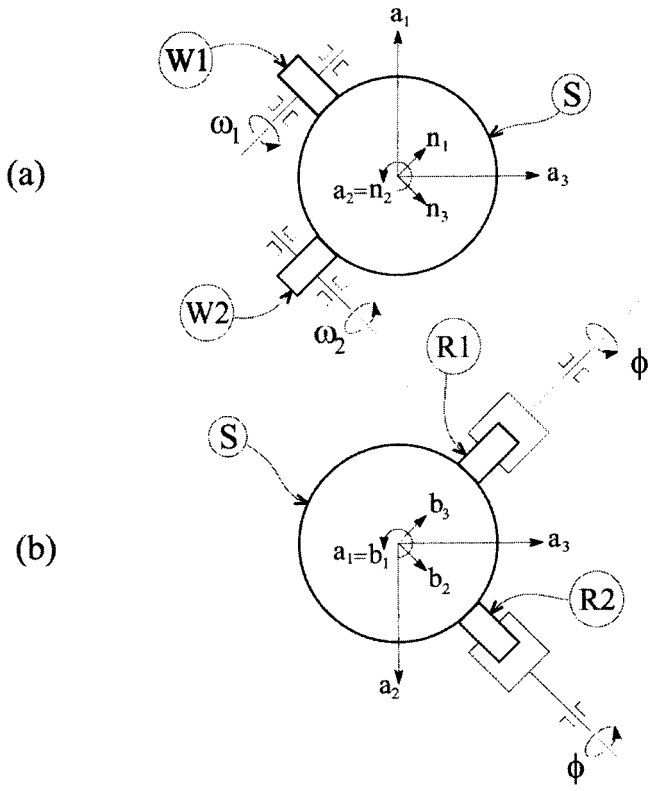

Fig. 3 Two views of the CVT with sphere *S* caged between drive rollers *W*1 and *W*2 and steering rollers *R*1 and *R*2.

3.1 Kinematics of the Ideal CVT. The angular velocities in N of rollers $W1$ and $W2$ are denoted ${}^N\boldsymbol{\omega}^{W1}$ and ${}^N\boldsymbol{\omega}^{W2}$, respectively. Let the scalars ω_1 and ω_2 be defined according to ${}^N\boldsymbol{\omega}^{W1} \triangleq -\omega_1\mathbf{n}_1$, ${}^N\boldsymbol{\omega}^{W2} \triangleq \omega_2\mathbf{n}_3$. Let the N-measure numbers of the angular velocity of S in N be defined as ${}^N\boldsymbol{\omega}^S \triangleq \Omega_1\mathbf{n}_1 + \Omega_2\mathbf{n}_2 + \Omega_3\mathbf{n}_3$. A rolling constraint equation may be written for the contact between S and $R1$

$${}^N\boldsymbol{\omega}^S \times R\mathbf{b}_3 = {}^N\boldsymbol{\omega}^{R1} \times -r\mathbf{b}_3, \tag{4}$$

while a second rolling constraint may be written for the contact between S and $R2$:

$${}^N\boldsymbol{\omega}^S \times R\mathbf{b}_2 = {}^N\boldsymbol{\omega}^{R2} \times -r\mathbf{b}_2. \tag{5}$$

Dot multiplication of these two vector equations with unit vectors $\mathbf{n}_i$ ($i = 1,2,3$) produces six scalar equations which may be manipulated to yield

$$\Omega_2 = 0, \tag{6}$$

or the axis of rotation of sphere S lies in the $\mathbf{n}_1 - \mathbf{n}_3$ plane (which contains the axes of $W1$ and $W2$). Secondly, the scalar equations yield

$$\frac{\Omega_3}{\Omega_1} = \frac{\tan(\phi) - \sqrt{2}}{\tan(\phi) + \sqrt{2}}. \tag{7}$$

A rolling constraint may be written for each of the drive rollers, and these two equations divided to yield an expression for the transmission ratio:

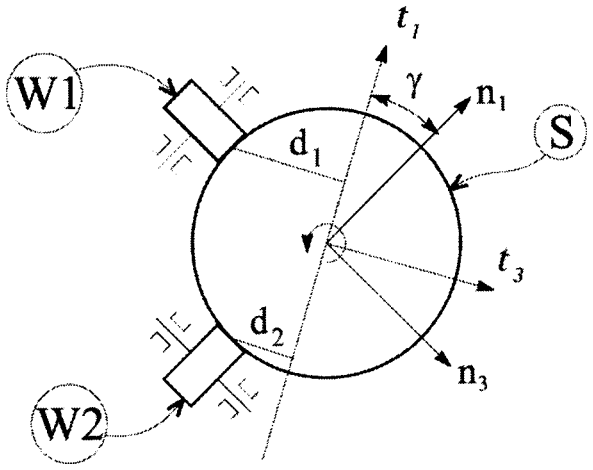

Fig. 4 The rotational axis of the sphere oriented by angle γ

$$\frac{\omega_2}{\omega_1} = -\frac{\Omega_3}{\Omega_1}, \tag{8}$$

which together with Eq. (7) gives a formula for the transmission ratio in terms of the steering angle ϕ

$$\frac{\omega_2}{\omega_1} = -\frac{\tan(\phi)-\sqrt{2}}{\tan(\phi)+\sqrt{2}}. \tag{9}$$

The ratio Ω_3/Ω_1, which is the common term between Eq. (7) and Eq. (8), orients the rotational axis of S in the $\mathbf{n}_1-\mathbf{n}_3$ plane. In summary, two rolling constraints at the steering rollers set this ratio, while an additional two ideal rolling constraints at the drive rollers relate this ratio to the ratio of speeds, ω_1/ω_2. We define γ as the angle subtended by the rotational axis of S (given by ${}^N\boldsymbol{\omega}^S = \Omega_1\mathbf{n}_1+\Omega_3\mathbf{n}_3$) and the unit vector $\mathbf{n}_1$, recognizing that

$$\tan\gamma = -\frac{\Omega_3}{\Omega_1} \tag{10}$$

Figure 4 explicitly shows the rotational axis of S drawn over the CVT view of Fig. 3(*a*) for an example γ value of about 30°. Note that trigonometry also reveals

$$\frac{\omega_2}{\omega_1} = \frac{d_2}{d_1} = \tan(\gamma), \tag{11}$$

where d_1 and d_2 are the perpendicular distance from each drive roller contact point to the rotational axis of S. Equation (11) is the transmission law relating angular speeds for the ideal CVT.

3.1.1 Force Balance. To construct the transmission law that relates the torques applied to the drive rollers, we may assume steady motion and balance internal forces in the CVT. In this idealized model, we assume that each rolling contact can transmit any force without consequence to its rolling constraint (no microslip (creep) or gross slip). Thus the torque applied to roller $W1$, $\boldsymbol{\tau}_1 = -\tau_1\mathbf{n}_1$, creates a friction force $\mathbf{F}_1 = \tau_1/r\mathbf{n}_2$ acting on S at the point located from the sphere center by the position vector $-R\mathbf{n}_3$. The torque applied to roller $W2$, $\boldsymbol{\tau}_2 = \tau_2\mathbf{n}_3$ creates a friction force $\mathbf{F}_2 = \tau_2/r\mathbf{n}_2$ acting on S at the point located from the sphere center by the position vector $-R\mathbf{n}_1$. Balancing the moments of $\mathbf{F}_1$ and $\mathbf{F}_2$ about the rotational axis of S ($\mathbf{t}_1$), we find

$$\frac{\tau_1}{\tau_2} = -\tan(\gamma) \tag{12}$$

Equation (12) is the transmission law relating torque measure numbers for the ideal CVT.

3.1.2 Coupling Space. In Section 2, the abstract space Σ, called coupling space, was introduced to illustrate the interpretation of the steered wheel as a transmission between two linear speeds. Likewise, a coupling space can be constructed for the rotational CVT and used to gain insight into both transmission laws: that relating speeds, Eq. (11) and that relating torques, Eq. (12). In their respective coupling spaces, the steered wheel and the CVT are completely analogous.

The unit vector $\boldsymbol{\sigma}_1$ of the reference basis Σ is associated with angular displacements of drive roller $W1$ and unit vector $\boldsymbol{\sigma}_2$ is associated with angular displacements of drive roller $W2$. Thus points in coupling space Σ correspond to various pairs of drive roller angular displacements while directions in coupling space are associated with various drive roller angular speed ratios. A reference basis U spanned by unit vectors $\mathbf{u}_\parallel$ and $\mathbf{u}_\perp$ may be set up to describe the allowed and disallowed directions in coupling space. Basis U is oriented with respect to basis Σ by the angle γ.

The angular speed ω_1 of $W1$ and the angular speed ω_2 of $W2$ are the Σ-measure numbers of a vector $\boldsymbol{\omega}$: $\boldsymbol{\omega} \triangleq \omega_1\boldsymbol{\sigma}_1+\omega_2\boldsymbol{\sigma}_2$ After defining the U-measure numbers of $\boldsymbol{\omega}$ using $\boldsymbol{\omega} \triangleq \omega_\parallel\mathbf{u}_\parallel+\omega_\perp\mathbf{u}_\perp$, we see that the transmission law relating speeds, Eq. (11), requires

$$\omega_\perp = 0 \tag{13}$$

A vector $\boldsymbol{\tau}$ may be defined in coupling space to characterize the torques applied to the drive rollers $W1$ and $W2$. Define the Σ-measure numbers of $\boldsymbol{\tau}$ using: $\boldsymbol{\tau} \triangleq \tau_1\boldsymbol{\sigma}_1+\tau_2\boldsymbol{\sigma}_2$ Also define U-measure numbers of $\boldsymbol{\tau}$ as follows: $\boldsymbol{\tau} \triangleq \tau_\parallel\mathbf{u}_\parallel+\tau_\perp\mathbf{u}_\perp$ Equation (12) reads in the U basis:

$$\tau_\parallel = 0. \tag{14}$$

The rotated bases Σ and U will prove very useful in discussions of the nonideal behavior of the CVT. The vectors $\boldsymbol{\omega}$ and $\boldsymbol{\tau}$ in coupling space encapsulate all functional aspects of the CVT. They are macro properties in the sense that they encompass the roller speeds or roller torques pairwise (rather than individually).

The magnitude of the vector $\boldsymbol{\tau}$ is $\tau_\perp$ by Eq. (14). It may be related to the torques τ_1 and τ_2 through:

$$\tau_1 = -\tau_\perp\sin(\gamma) \quad \tau_2 = \tau_\perp\cos(\gamma) \tag{15}$$

Under conditions of steady motion, the CVT may transmit a torque from one drive roller to the other. Traction forces at each drive roller develop to support this transmitted torque. In coupling space, the transmitted torque is interpreted as a torque $\tau_\perp$ in the disallowed direction. In the ideal transmission, any $\tau_\perp$ value may be transmitted without consequence to the transmission law relating angular speeds. This is not true in the non-ideal CVT, as we explore below.

4 The Nonideal Wheel

If a lateral load is applied during rolling, the wheel will drift laterally as it rolls ahead. Its actual velocity $\mathbf{v}$ will make an angle α, known as the sideslip angle, with the wheel heading $\mathbf{b}_1$. Lateral creep ξ_y, defined as the ratio of the lateral speed $v_\perp$ to the absolute value of the rolling speed $v_\parallel$, is related to the sideslip angle as follows:

$$\xi_y \triangleq \frac{v_\perp}{|v_\parallel|} = \tan(\alpha). \tag{16}$$

A relationship between sideslip angle α and applied lateral force $F_\perp$ may be constructed by considering radial and axial deformations in an elastic wheel that give rise to a curvilinear contact line against the rolling surface comprising a linear sticking region and a curving slipping region. The sideslip angle dictates the direction of the linear region with respect to the heading while in the slipping region, the accumulated stresses relax. Across the sticking region, static friction will apply while across the slipping region, kinetic friction will apply. Integrating across the entire contact line, one arrives at an expression for the lateral force. One

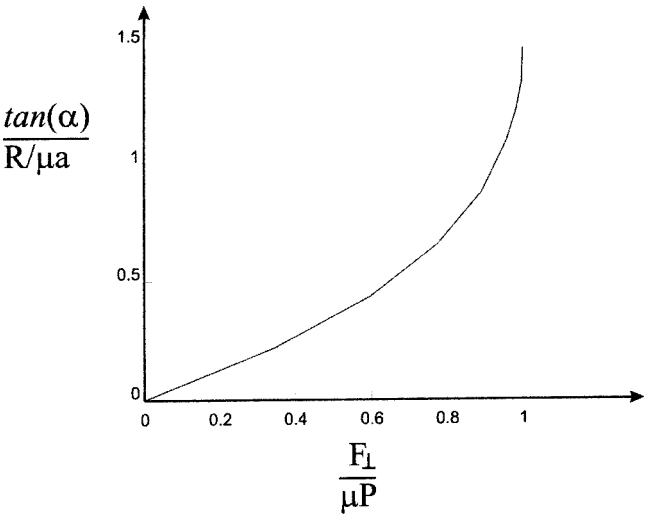

Fig. 5 The sideslip angle α predicted by the elastic model in response to an applied lateral force $F_\perp$

such relationship (See [6]) is shown in Fig. 5. The tangent of the sideslip angle, normalized by $R/\mu a$, is plotted versus the nondimensionalized lateral force $F_\perp/\mu P$, where R is the wheel radius, a is the contact line half-width, μ is the coefficient of friction, and P is the normal foce. Note that for small sideslip angles, the relationship between sideslip angle and disallowed force is approximately linear. The slope C of the linear portion is called cornering stiffness in tire mechanics. Past a certain sideslip angle, the Wheel's ability to support lateral forces breaks down until the entire contact line is in slip.

5 The Nonideal CVT

Like the Wheel, a physically realizable CVT cannot strictly prevent motion in the disallowed direction. Under a disallowed force, the rolling constraints at the drive rollers give way to creep. In contrast to the Wheel, where lateral traction supports a disallowed force, in the CVT it is *longitudinal* traction that supports a disallowed force. Moreover, there are two longitudinal tractions in the CVT: one at each drive roller. Associated with this pair of longitudinal tractions is a pair of longitudinal creeps. In coupling space, this pair of longitudinal creeps may be interpreted as a single lateral creep or expressed as a sideslip angle. But before we consider the longitudinal creeps as a pair in coupling space, we must consider them individually in physical space.

In contrast to *lateral* traction and creep, an elastic model is not required to express longitudinal creep as a function of longitudinal traction so long as two conditions are met. First, spin must be present. That is, the two rolling bodies must have a relative angular velocity with non-zero component in the contact normal direction. Second, the two rolling bodies must contact at more than a single point. Both of these conditions are met in a rigid cylindrical wheel turning a corner while rolling on a plane. Both conditions are also met in a rigid cylindrical wheel rolling on a cone.

When spin is nonzero, there is only one point of the contact patch in rolling; the remaining portions of the contact patch must be in sliding. Sliding is in one direction on one side of the rolling point and in the other direction on the other side. After representing the sliding in a relative velocity field, the traction transmitted across the contact patch can be computed as the vector sum of the friction force acting at each point in the contact patch. If a braking axial torque is applied (balanced by traction on the wheel opposite the direction of rolling,) the point of rolling will migrate toward the center of rotation, whereas if an accelerating axial torque is applied (balanced by traction on the wheel in the direction of rolling,) the rolling point will migrate away from the center of rotation. Any deviation of the rolling point away from the center of the contact line produces a longitudinal creep.

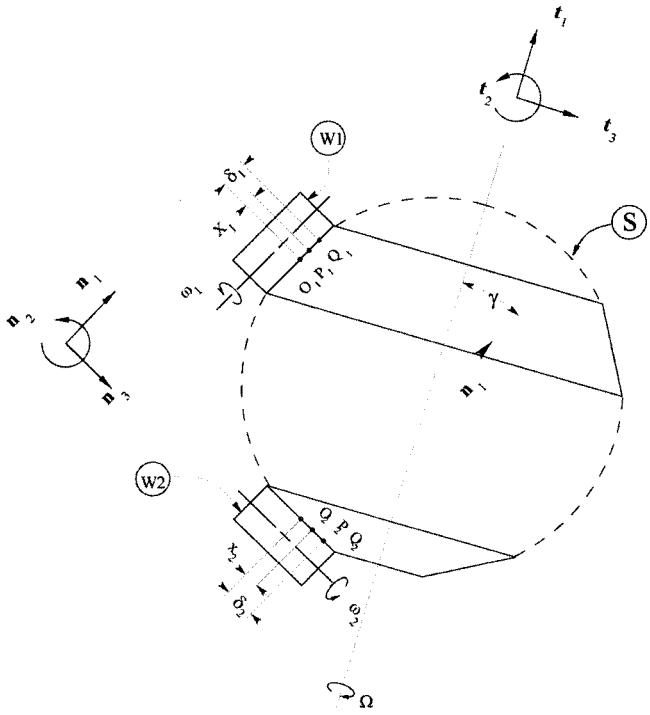

Fig. 6 Model of the CVT, with sphere *S* represented by two coaxial cones making line contact with drive rollers *W*1 and *W*2

In the following, we will construct a rigid body model of the CVT that accounts for longitudinal creep in each of the drive rollers. The drive rollers of the CVT meet the first condition for creep, since spin is indeed present in the contact patch between each drive roller and the sphere. Each drive roller is in a state of cornering, with the cornering radius established by the transmission ratio. In fact (see Fig. 4), as the transmission ratio approaches zero, the axis of rotation of the sphere approaches the center of one of the contact patches, causing the cornering radius for that roller to approach zero and the cornering radius of the other roller to approach infinity. As the transmission ratio approaches infinity, the situation for the two drive rollers is reversed. Insofar that creep is a function of cornering radius, we expect to see a dependence of the CVT transmission law for speeds on the transmitted load. Further, we expect that this dependence will vary as a function of the steering angle setting (the transmission ratio setting) and wish to quantify this dependence.

The second requirement for the development of creep in rolling rigid bodies is met if the bodies make line contact. Line contact is not possible between rigid cylindrical rollers and a rigid sphere, so we modify the geometric model of the CVT as described in section 5.1.

5.1 Kinematics of the Nonideal CVT. Line contact is set up between the sphere and each of the rollers by modeling the sphere as a pair of connected co-axial cones. Figure 6 shows the system S comprising two cone sections. The vertex angle of each cone is chosen so that line contact is established between S and drive rollers $W1$ and $W2$. Note that the vertex angles vary as γ varies. A reference basis T of unit vectors $\mathbf{t}_i$ $(i=1,2,3)$ is used to locate the rotational axis of S as follows: basis T is first aligned with N and then subjected to a right-hand rotation about $\mathbf{n}_2$ through the angle γ. System S rotates with an angular speed Ω about unit vector $\mathbf{t}_1$, or ${}^N\boldsymbol{\omega}^S=\Omega\mathbf{t}_1$. Drive rollers $W1$ and $W2$,

both of radius r and width $2a$, roll on the cones of S. As before, the axis of drive roller $W1$ is aligned with $\mathbf{n}_1$ and the axis of drive roller $W2$ is aligned with $\mathbf{n}_3$.

The angle γ is set by the steering angle ϕ of the steering rollers according to Eq. (9). We assume that the steering rollers are able to maintain the orientation of the axis of the sphere, without dependence on the traction forces developed at the drive rollers. This assumption is based on the fact that the traction forces at the drive rollers have no moment about $\mathbf{n}_2$, and therefore no influence over the rotation of basis T (which locates the rotational axis of S) about $\mathbf{n}_2$.

Define the center of each contact patch as point O_i $(i=1,2)$. Additionally, as shown in Fig. 6, a generic point P_i is located a distance x_i from O_i and a special point Q_i is located a distance δ_i away from O_i $(i=1,2)$. Point Q_i $(i=1,2)$, called the rolling point, is used to identify the unique position in each contact patch at which the relative velocity is zero. Measure numbers for the angular velocity ${}^N\boldsymbol{\omega}^S$ of S in N, the angular velocity ${}^N\boldsymbol{\omega}^{W1}$ of $W1$ in N, and the angular velocity ${}^N\boldsymbol{\omega}^{W2}$ of $W2$ in N are defined as follows:

$$
\begin{aligned}
{}^N\boldsymbol{\omega}^S &= \Omega \mathbf{t}_1 \\
{}^N\boldsymbol{\omega}^{W1} &= -\omega_1 \mathbf{n}_1 \\
{}^N\boldsymbol{\omega}^{W2} &= \omega_2 \mathbf{n}_3
\end{aligned}
\tag{17}
$$

Let us first develop the relative velocity field for each contact line in terms of creep and spin. Subsequently, we will find the resultant tractive force by application of the Coulomb law and integration. Additionally, we will find the traction torque by integration. We begin with the contact line between $W1$ and S.

The relative velocity at the generic point P may be expressed

$$
\Delta\mathbf{v}^{P1} = \boldsymbol{\omega}^{W1} \times (r\,\mathbf{n}_3 + x_1\,\mathbf{n}_1) - \boldsymbol{\omega}^S \times (-R\,\mathbf{n}_3 + x_1\,\mathbf{n}_1). \tag{18}
$$

After rearranging terms and defining the relative velocity at O as $\Delta\mathbf{v}^{O1}$ and the relative angular velocity between $W1$ and S as $\Delta\boldsymbol{\omega}_1 = \boldsymbol{\omega}^{W1} - \boldsymbol{\omega}^S$, one finds

$$
\Delta\mathbf{v}^{P1} = \Delta\mathbf{v}^{O1} + \Delta\boldsymbol{\omega}_1 \times x_1\,\mathbf{n}_1 \tag{19}
$$

That is, the *relative* velocity field in the contact patch may be characterized as a rigid body motion. A similar vector expression holds for the contact patch between $W2$ and S. Once the cross product has been carried out, all vectors are in the $\mathbf{n}_2$ direction, and the subscripts 1 or 2 may be dropped.

After defining $\Delta\omega \triangleq \Delta\boldsymbol{\omega}\cdot\mathbf{n}_3$, and noting that $\Delta\mathbf{v}^P$ and $\Delta\mathbf{v}^O$ have only $\mathbf{n}_2$ measure numbers (which are denoted without boldface), we have:

$$
\Delta v^P \mathbf{n}_2 = \Delta v^O \mathbf{n}_2 + \Delta\omega\, x\, \mathbf{n}_2. \tag{20}
$$

To nondimensionalize the terms in this equation, the absolute value of the common speed $|v^Q|$ at Q is chosen, where Q is the rolling point. Equation (20) may be dot multiplied by $\mathbf{n}_2$ and divided through by $|v^Q|$ to yield:

$$
\frac{\Delta v^P}{|v^Q|} = \frac{\Delta v^O}{|v^Q|} + \frac{\Delta\omega a}{|v^Q|}\,\frac{x}{a} \tag{21}
$$

The left hand side we define as the slip $\lambda(x)$ at the point P of the contact patch. The first term on the right hand side we define as longitudinal creep ξ and the factor $\Delta\omega a/|v^Q|$ in the last term we define as spin ψ. Recall that a is the contact line half-width. We now have an expression for the slip at a generic point in the contact patch in terms of the bulk properties creep ξ and spin ψ:

$$
\lambda(x) = \xi + \psi\frac{x}{a} \tag{22}
$$

This expression describes the slip in the contact patch between $W1$ and S and between $W2$ and S. To particularize the expression for each contact patch, the subscripts 1 and 2 may be used with ξ, ψ, λ, and x.

We now derive the creep and spin parameters for each roller. A rolling constraint at the point Q_1 produces the constraint equation

$$
\omega_1 r = \Omega(\cos(\gamma)R - \sin(\gamma)\delta_1). \tag{23}
$$

Applying the definitions of ξ and ψ and making use of Eq. (23),

$$
\xi_1 = \frac{-\delta_1 \sin(\gamma)}{|R\cos(\gamma) - \delta_1 \sin(\gamma)|} \tag{24}
$$

$$
\psi_1 = \frac{\sin(\gamma)a}{|R\cos(\gamma) - \delta_1 \sin(\gamma)|} \tag{25}
$$

Likewise, a rolling constraint at the point Q_2 produces

$$
\omega_2 r = \Omega(\sin(\gamma)R - \cos(\gamma)\delta_2). \tag{26}
$$

The creep and spin at roller 2 in terms of γ and δ_2 are

$$
\xi_2 = \frac{-\delta_2 \cos(\gamma)}{|R\sin(\gamma) - \delta_2 \cos(\gamma)|} \tag{27}
$$

$$
\psi_2 = \frac{-\cos(\gamma)a}{|R\sin(\gamma) - \delta_2 \cos(\gamma)|} \tag{28}
$$

Dividing Eqs. (26) and (23), we have

$$
\frac{\omega_1}{\omega_2} = \frac{\cos(\gamma) - \dfrac{1}{R}\delta_1 \sin(\gamma)}{\sin(\gamma) - \dfrac{1}{R}\delta_2 \cos(\gamma)}. \tag{29}
$$

The variables δ_1 and δ_2 may be replaced by ratios of the creep and spin parameters using Eqs. (24), (25), (27), and (28), giving:

$$
\frac{\omega_1}{\omega_2} = \frac{\cos(\gamma) + \dfrac{a}{R}\dfrac{\xi_1}{\psi_1}\sin(\gamma)}{\sin(\gamma) - \dfrac{a}{R}\dfrac{\xi_2}{\psi_2}\cos(\gamma)}. \tag{30}
$$

Equation (30) is the non-ideal transmission law relating angular speeds. It expresses the ratio of angular speeds as a function of the creep to spin ratios at each drive roller, which in turn are functions of the tractions transmitted across each contact patch. We are now ready to develop the dependence of creep and spin on the tractive forces.

5.2 Force Balance for the Non-ideal CVT. In section 3.1.1, we assumed that any tractive force could be transmitted across the contacts between drive rollers and sphere, without consequence to the rolling constraints. This assumption no longer holds in the present section, where we treat the nonideal CVT. Now the tractive force affects the rolling constraints, giving rise first (at low magnitudes) to longitudinal creep and eventually to gross longitudinal slip.

Our present objective is to relate the creep and spin parameters to the tractive force at each contact patch. This can be done by appealing to Eq. (22) and applying the law of Coulomb friction. Equation (22) gives the slip at a point located by x in a contact patch whose velocity field is characterized by ξ and ψ. Note that $\lambda(x)$ (the slip at P) and Δv^P (the relative velocity at P) have the same sign, so λ may be used to form a vector expression for the friction force acting on the sphere (from the roller) at point P, whose direction may be expressed with respect to a fixed reference basis. The friction force acting on S across a differential element of the contact patch is given by the Coulomb law:

$$
d\mathbf{f} = \mu\frac{N}{2a}\,\mathrm{sgn}(\lambda(x))\,\mathbf{n}_2 \tag{31}
$$

Table 1 Integration results

case	limits	$\frac{F}{\mu N}$	$\frac{M}{a\mu N}$
I	$\xi+\psi>0$ $\xi-\psi<0$	$\frac{\xi}{\psi}$	$\frac{1}{2}\left(1-(\frac{\xi}{\psi})^2\right)$
II	$\xi+\psi<0$ $\xi-\psi>0$	$-\frac{\xi}{\psi}$	$-\frac{1}{2}\left(1-(\frac{\xi}{\psi})^2\right)$
III	$\xi+\psi>0$ $\xi-\psi>0$	1	0
IV	$\xi+\psi<0$ $\xi-\psi<0$	−1	0

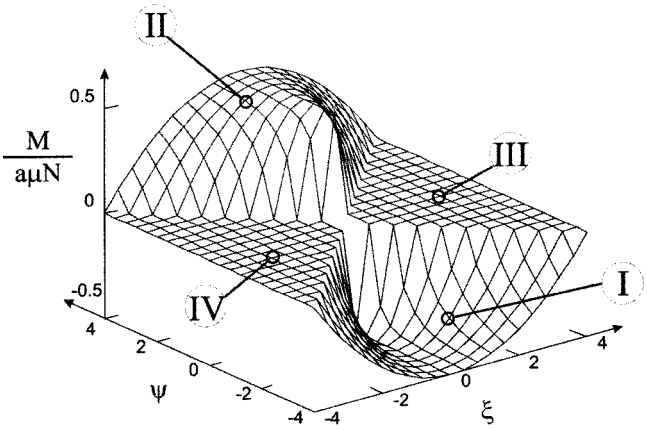

Fig. 8 Torque as a function of creep ξ and spin ψ

where N is the normal force between S and each drive roller. Integrating across the contact patch,

$$\frac{\mathbf{F}}{\mu N}=\frac{1}{2a}\int_{-a}^{a}\operatorname{sgn}(\lambda(x))\,\mathbf{n}_2 dx=\frac{1}{2a}\int_{\xi-\psi}^{\xi+\psi}\operatorname{sgn}(\lambda)\frac{a}{\psi}d\lambda\;\mathbf{n}_2, \tag{32}$$

where the change of variables according to Eq. (22) was used. In similar fashion, an integral expression for the tractive torque $\mathbf{M}$ about $\mathbf{n}_1$ (for $W1$) may be found as a function of λ:

$$\frac{\mathbf{M}}{a\mu N}=\frac{1}{2a^2}\int_{\xi-\psi}^{\xi+\psi}(\lambda-\xi)\operatorname{sgn}(\lambda)\,d\lambda\;\mathbf{n}_1 \tag{33}$$

The direction of $\mathbf{M}$ for $W2$ is $\mathbf{n}_3$. To evaluate these integrals, we delineate four cases, depending on the sign of the integration limits (the sum and difference of creep and spin). Results are given in Table 1.

Note that the relationship between creep and spin at a contact patch and the associated tractive force is quite simple and symmetric. The non-dimensionalized tractive force $F/\mu N$ is plotted against ξ and ψ in Fig. 7. The non-dimensionalized traction torque $M/a\mu N$ is plotted against ξ and ψ in Fig. 8. Each of the four regions, divided by the planes $\xi=\psi$ and $\xi=-\psi$, have been noted in Figs. 7 and 8.

Table 1 gives the desired relationship between the creep and spin parameters and the tractive force. Cases I and II account for creep whereas cases III and IV describe limiting friction (gross slip). Although it was constructed by expressing the traction force in terms of ξ and ψ, Table 1 can also be used in the reverse direction, to express the ratio of ξ to ψ in terms of the traction force. This is how Table 1 will be used in our study of the kinetics of the CVT in the following section.

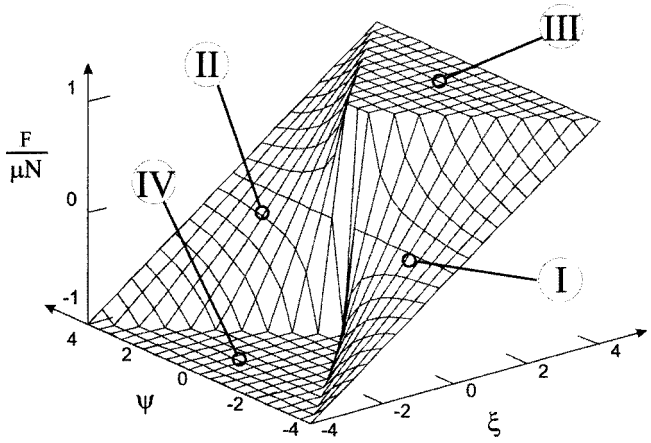

Fig. 7 Normalized tractive force versus creep ξ and spin ψ

We now balance the forces $\mathbf{F}_1$ and $\mathbf{F}_2$ in the CVT. For steady motion, the tractive forces $\mathbf{F}_1$ and $\mathbf{F}_2$ must not accelerate S. That is, their moments about $\mathbf{t}_1$, the rotational axis of S, must cancel one another. Note that the tractive forces $\mathbf{F}_1$ and $\mathbf{F}_2$ are balanced on each drive roller by the applied axial torques $\boldsymbol{\tau}_1=-\tau_1\mathbf{n}_1$ and $\boldsymbol{\tau}_2=\tau_2\mathbf{n}_3$: $\tau_1/r=F_1$ and $\tau_2/r=F_2$. If we assume that the resultant traction forces act at the center of the contact lines and if we neglect the traction torques,[1] the sum of moments of the traction forces yields

$$\frac{\tau_2}{\tau_1}=-\frac{1}{\tan(\gamma)} \tag{34}$$

This is the same as the transmission law relating torques in the ideal CVT. Thus, neglecting the traction torques, the transmission law relating torques does not deviate from its ideal.

Let us associate the drive and load on the CVT with the axial torques $\boldsymbol{\tau}_2$ and $\boldsymbol{\tau}_1$, respectively. Together $\boldsymbol{\tau}_2$ and $\boldsymbol{\tau}_1$ are the load transmitted through the CVT. By Eq. (15) in Section 3.1.1, we have: $\tau_1=-\tau_\perp\sin(\gamma)$ and $\tau_2=\tau_\perp\cos(\gamma)$ The angle γ still defines the direction for $\boldsymbol{\tau}_\perp$.

5.3 Kinetics of the Nonideal CVT. We are now ready to couple the transmission law relating angular speeds, Eq. (30), to the transmission law relating torque measure numbers, Eq. (34), through the application of Table 1. The only complication is presented by the four cases of Table 1 that account for limiting friction. The situation can be handled by considering γ in increments of $\pi/2$, for the quadrant in which γ falls determines the sign of ψ_1 and ψ_2, which allows one to differentiate cases I and II in Table 1. The boundaries of cases III and IV can be differentiated if γ is further subdivided into sectors of $\pi/4$.

Figure 9 shows the governing relationships, laid out graphically around a circle to indicate the range of γ in which they are valid. The sign of ψ_i $(i=1,2)$, indicated in the innermost ring of Fig. 9, is constructed with reference to Eqs. (25) and (28). The relationship between tractive torque and the creep to spin ratio is constructed with reference to Table 1 and given in the intermediate ring of Fig. 9. Considering γ in increments of $\pi/2$, the normalized torques can be substituted for the creep to spin ratios in Eq. (30). However, having identified $W2$ as the drive and $W1$ as the driven wheel, we must incorporate a dependence on γ of the sign on the

[1]Note that in this discussion we have neglected the contribution of the traction torques to the moment balance on S. The contribution of the traction torques is quite small in comparison to that of the tractive forces, especially when the contact patches are small.

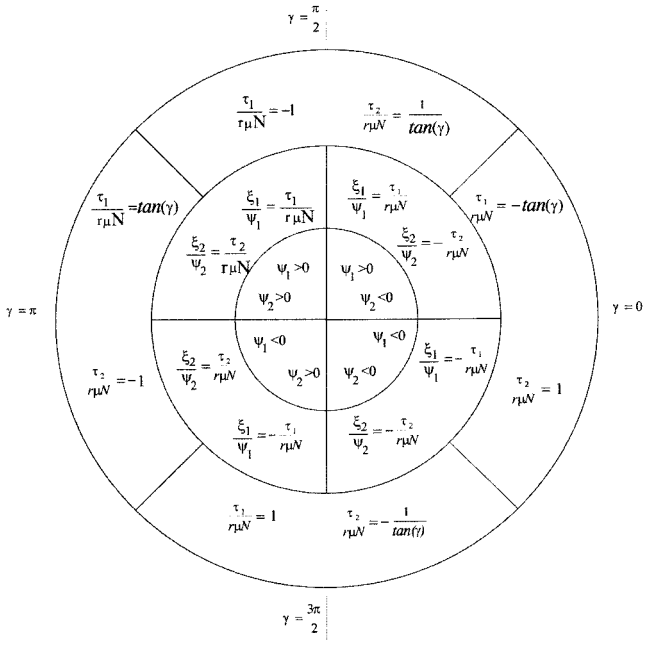

Fig. 9 The governing relationships are drawn graphically around a circle so as to indicate the range of γ in which they are valid. In concentric regions starting at the center, the signs of the spin parameters, the relationships between the creep to spin ratios and the drive roller torques, and the drive roller torque values at limiting friction are noted.

second term in both the numerator and denominator of Eq. (30) to ensure that the CVT acts as a dissipative element:

$$\frac{\omega_1}{\omega_2}=\frac{\cos(\gamma)+\mathrm{sgn}(\tan(\gamma))\,\frac{a}{R}\,\frac{\xi_1}{\psi_1}\sin(\gamma)}{\sin(\gamma)-\mathrm{sgn}(\tan(\gamma))\,\frac{a}{R}\,\frac{\xi_2}{\psi_2}\cos(\gamma)}. \tag{35}$$

This dependence will ensure that the projections of $\boldsymbol{\omega}=\omega_\perp \mathbf{u}_\perp+\omega_\parallel \mathbf{u}_\parallel$ and $\boldsymbol{\tau}=\tau_\perp \mathbf{u}_\perp$ on $\boldsymbol{\sigma}_1$ and $\boldsymbol{\sigma}_2$ obey the law: $\mathrm{sgn}(\omega_2\tau_2)=-\mathrm{sgn}(\omega_1\tau_1)$, which ensures that power to the CVT flows in opposite directions on either drive roller. In effect, we have reversed the direction of $\boldsymbol{\tau}$ when $\mathbf{u}_\parallel$ has positive directions in quadrants II and III of Σ-space and reversed the direction of $\boldsymbol{\omega}$ when $\mathbf{u}_\parallel$ has positive directions quadrants III and IV. This allows us to employ our analysis that made use of the rotation of the U basis relative to the Σ basis to describe our CVT (consistent with $\omega_1/\omega_2=1/\tan(\gamma)$, $\tau_2/\tau_1=-1/\tan(\gamma)$), while constructing relationships that refer to the traditional input-output identified transmission laws $\omega_1/\omega_2=\tau_2/\tau_1=1/\tan(\gamma)$ when evaluating its performance.

So, considering γ in increments of $\pi/2$, the nondimensionalized torques can be substituted for the creep to spin ratios in Eq. (35). Then Eq. (34) can be used to obtain an expression for the speed ratio ω_2/ω_1 in terms of the torque load $\tau_\perp$. For example, for $0<\gamma<\pi/2$:

$$\frac{\omega_1}{\omega_2}=\frac{\cos(\gamma)-\frac{a}{R}\,\frac{\tau_\perp}{r\mu N}\sin^2(\gamma)}{\sin(\gamma)+\frac{a}{R}\,\frac{\tau_\perp}{r\mu N}\cos^2(\gamma)} \tag{36}$$

For $-\pi/2<\gamma<0$,

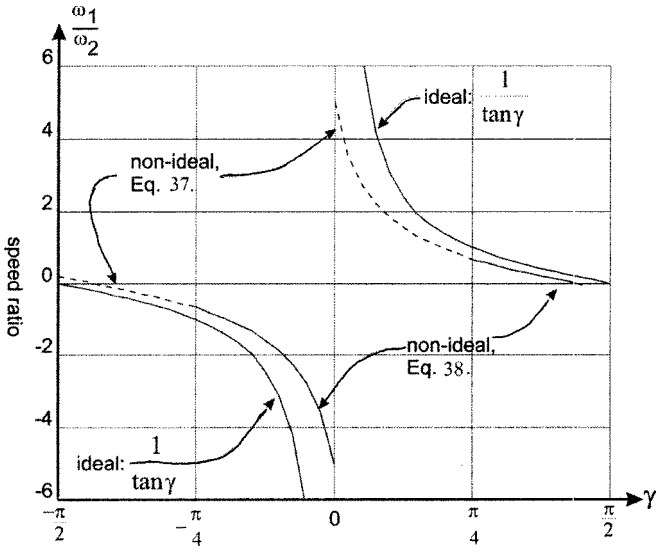

Fig. 10 The transmission ratio of speeds as a function of the transmission angle γ with $a/R=0.2$

$$\frac{\omega_1}{\omega_2}=\frac{\cos(\gamma)+\frac{a}{R}\,\frac{\tau_\perp}{r\mu N}\sin^2(\gamma)}{\sin(\gamma)+\frac{a}{R}\,\frac{\tau_\perp}{r\mu N}\cos^2(\gamma)} \tag{37}$$

These expressions hold so long as the slip is not all in the same direction, in either contact line.

Beyond a certain $\tau_\perp$, which will itself be a function of γ, there will be no more available tractive force in one or the other drive rollers. At that time, the normalized tractive force at that roller will be unity, the slip will be in the same direction across the entire contact patch, and equivalently, the rolling point Q will be at the edge of that contact patch. With a disallowed force $\tau_\perp$ which increases beyond that point, the sideslip angle will increase unchecked and there will be acceleration in the disallowed direction. To find the limits of performance, the creep and spin variables are particularly handy, since the borderline cases are symmetric in $\xi-\psi$ space. Let us call the traction associated with slip all in the same direction within a contact line "limiting traction."

Whether limiting traction is attained first at roller $W1$ or $W2$ depends on the angle γ. Since $\cos(\gamma)>\sin(\gamma)$ for $0<\gamma<\pi/4$, by Eq. (34) roller $W2$ will first attain the limit $\tau_2/r\mu N=1$ and by Eq. (34), $\tau_1/r\mu N=-\tan(\gamma)$, as noted in the outermost ring in Figure 9. Together with the traction torque and creep to spin ratio relationships for $0<\gamma<\pi/2$ (Eq. (35) and the intermediate ring of Table 9), these limiting values give

$$\frac{\omega_1}{\omega_2}=\frac{c^2\gamma-\frac{a}{R}s^2\gamma}{s\gamma c\gamma+\frac{a}{R}c^2\gamma} \tag{38}$$

where $c\gamma$ denotes $\cos(\gamma)$ and $s\gamma$ denotes $\sin(\gamma)$. For $\pi/4<\gamma<\pi/2$, roller $W1$ first attains the limit and

$$\frac{\omega_1}{\omega_2}=\frac{c\gamma s\gamma-\frac{a}{R}s^2\gamma}{s^2\gamma+\frac{a}{R}c^2\gamma}. \tag{39}$$

Analogous considerations lead to similar expressions for the remaining $\pi/4$ sectors of γ. Figure 10 shows the speed ratio ω_1/ω_2 at limiting traction as a function of the CVT steering angle γ when

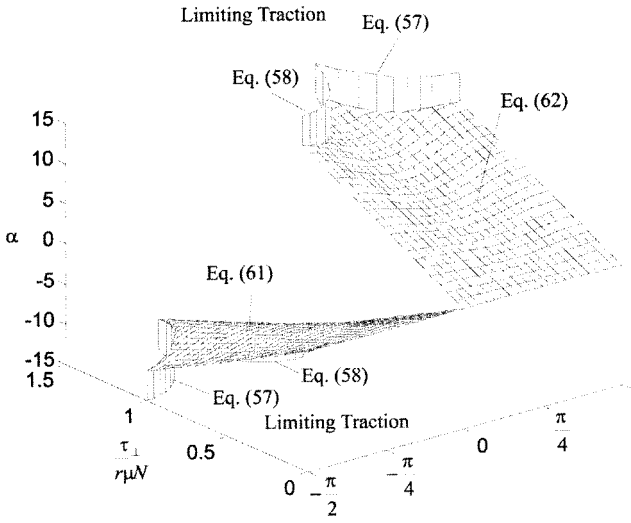

Fig. 11 Sideslip angle α as a function of the disallowed force $\tau_\perp$ and the transmission angle γ. Beyond the limiting curve, α will increase without regard to $\tau_\perp$ applied.

$a/R=0.2$. The nonideal case at limiting traction is given by Eqs. (38) and (39) for $0<\gamma<\pi/2$. The ideal case $1/\tan(\gamma)$ is also shown for comparison.

Figure 10 may be interpreted in terms of the question posed in the introduction, whether the ability of the CVT to transmit loads is compromised when spin dominates in one contact line or the other. We see that indeed, the ability to maintain the speed ratio setting $1/\tan(\gamma)$ breaks down when transmitting non-zero loads $\tau_\perp$ for γ close to $n\pi/2,(i=0,1,2\ldots)$. At $\gamma=0$ and under limiting friction a maximum transmission ratio of about 5 is achieved when approaching from $\gamma>0$ and -5 when approaching from $\gamma<0$ rather than the ideal $+\infty$ and $-\infty$. Presumably other effects such as elasticity would contribute to a softening of the transition through zero in the region $\gamma=0$. As γ increases, the decreasing speed ratio attains zero at a value significantly lower than the ideal $\gamma=\pi/2$ and as γ decreases, the increasing speed ratio attains zero at a value significantly higher than the ideal $\gamma=-\pi/2$. For a significant region around $\gamma=\pm\pi/2$, there is no motion at the output shaft: $\omega_1=0$. Physically, the rolling point Q changes abruptly from one side of the contact line to the other under the drive roller $W2$ around $\gamma=0$. The position of the rolling point Q is ambiguous under the driven roller $W1$ in the region $\gamma=\pm\pi/2$.

We are ready to express the sideslip angle α as a function of the transmission load $\tau_\perp$ for the CVT. The sideslip angle is defined in coupling space as the angle between the heading (determined by the transmission ratio $\tan(\gamma)$) and the actual motion (whose measure numbers are ω_1 and ω_2). Thus α is available from the ratio of drive roller angular speeds:

$$\tan(\alpha+\gamma)=\frac{\omega_2}{\omega_1} \tag{40}$$

Using the trigonometric identity

$$\tan(\alpha+\gamma)=\frac{\tan(\alpha)+\tan(\gamma)}{1-\tan(\alpha)\tan(\gamma)} \tag{41}$$

and the expression (35) with Eq. (40) we can solve for α as a function of $\tau_\perp$ and γ. For $0<\gamma<\pi/2$,

$$\tan(\alpha)=\frac{\dfrac{a}{R}\dfrac{\tau_\perp}{r\mu N}(s^3\gamma+c^3\gamma)}{1+\dfrac{a}{R}\dfrac{\tau_\perp}{r\mu N}(c^2\gamma s\gamma-s^2\gamma c\gamma)} \tag{42}$$

And for $\pi/2<\gamma<\pi$ in similar fashion, but using

$$\tan(\alpha-\gamma)=\frac{\tan(\alpha)-\tan(\gamma)}{1+\tan(\alpha)\tan(\gamma)},$$

$$\tan(\alpha)=\frac{\dfrac{a}{R}\dfrac{\tau_\perp}{r\mu N}(s^3\gamma-c^3\gamma)}{1+\dfrac{a}{R}\dfrac{\tau_\perp}{r\mu N}(c^2\gamma s\gamma+s^2\gamma c\gamma)} \tag{43}$$

The sideslip angle is plotted in Fig. 11 as a function of the disallowed torque $\tau_\perp$ and the transmission angle γ for the range $-\pi/2<\gamma<\pi/2$. The remaining two quadrants of γ are essentially copies of this graph with similar discontinuities at $\gamma=n\pi/2,(n=0,1,2\ldots)$. Equations (42) and (43) were used to plot the upward sloping surface. Eqs. (38) and (39) with Eq. (41) were used to locate the limiting friction curve, shown as a curved vertical fence in Fig. 11.

This figure shows neatly that α is a nearly linear function of $\tau_\perp$ with a slope that is a weak function of γ. The highest value of $\tau_\perp$ attained before gross slip occurs is a function of γ with minima of $\tau_\perp=1$ at $\gamma=n\pi/2$ and maxima of $\tau_\perp=\sqrt{2}$ at $\gamma=\pi/4+n\pi/2$ $(n=0,1,2,3)$. Values of α increase with increasing $\tau_\perp$ for $0<\gamma<\pi/2$ but decrease with increasing $\tau_\perp$ for $-\pi/2<\gamma<0$, consistent with the dissipative property of the CVT.

As anticipated by intuition, the sideslip for a given $\tau_\perp$ is greater at $\gamma=n\pi/2$, $(n=0,1,2\ldots)$ when the rotational axis of S intersects one of the contact lines and the limiting value of $\tau_\perp$ is lower. Further, at these transmission ratios, the sideslip angle undergoes a reversal in sign to account for the power sign convention (the changing roles of drive and driven rollers that ensure dissipativity). Indeed the feared breakdown that intuition had suggested does exist. Null and infinity transmission ratios are not achievable in the non-ideal case.

6 Summary

In this paper, we have developed the kinetics of the wheel and the CVT, illustrating the mechanism in each device by which the transmission law relating speeds becomes coupled to that relating forces. To describe deviation from the ideal rolling constraint, we used kinematic creep. Viewed in coupling space, both the Wheel and the CVT are subject to *lateral* creep when a force is applied in the disallowed direction. In physical space, however, the wheel supports a disallowed force with lateral traction and is subject to lateral creep, whereas the CVT supports a disallowed force (pair of drive roller torques) with a pair of longitudinal tractions and is subject to a pair of longitudinal creeps. The fact that the tractions are transmitted across contacts that undergo spin whose magnitude is again related to the transmission ratio makes the longitudinal creeps transmission ratio dependent in addition to load dependent. The pair of longitudinal creeps in the CVT, when viewed in coupling space, is interpreted as lateral creep. To express lateral creep in the Wheel as a function of lateral traction, an elastic model is used. To express the longitudinal creeps in the CVT as a function of longitudinal tractions, a rigid body model suffices, so long as the rolling bodies make line contact. An approximating physical model (two coaxial cones in place of the spherical rolling surface) was used to set up line contact.

Analytical expressions relating tractive force to creep and spin at each of two line contacts were incorporated into a full kinetostatic model of the CVT to yield the dependence of the speed ratio on the transmitted load and transmission ratio setting. Deviations from the ideal rendered very high transmission ratios unattainable and very low difficult to regulate. However, an approximately

linear relationship between sideslip angle and transmitted load is confirmed for the full range of transmission ratio settings.

These wheel and CVT models may be used to create model-based controllers for cobots that compensate for the effects of sideslip by counter-steering. Sideslip in the CVT causes a guiding surface to give way as an operator pushes against it. Counter-steering as a function of transmission ratio setting and applied load would restore the guiding surface. Although, according to the models presented here, only limited compensation may be provided, especially in the regions of very high or very low transmission ratios. Extensions to the models presented here include the addition of the elastic features of the Wheel model to the CVT model. In such an elastic model, the cones replacing the sphere will be unnecessary, and the effects of an elliptical contact patch may be explored.

Acknowledgments

The authors gratefully acknowledge the support of General Motors Corporation and the National Science Foundation under the postdoctoral program award No. 9625756.

References

[1] Colgate, J. E., Peshkin, M. A., and Wannasuphoprasit, W. 1996, ''Passive Robots and Haptic Displays Based on Nonholonomic Elements,'' *Proceedings, IEEE International Conference on Robotics and Automation*, Philidephia, PA.
[2] Peshkin, M. A., Colgate, J. E., Wannasuphoprasit, W., Moore, C. A., Gillespie, R. B., and Akella, P., 2001, ''Cobot Architecture,'' IEEE Trans. Rob. Autom., **17**(4), pp. 377–390.
[3] Liu, C., and Paul, B., 1989, ''Fully Developed Sliding of Rough Surfaces,'' ASME J. Tribol., **111**, pp. 445–451.
[4] Wang, B.-T., and Fries, R. H., 1989, ''Determination of Creep Force, Moment, and Work Distribution in Rolling Contact With Slip,'' ASME J. Tribol., **111**, 711–718.
[5] Howe, R. D., and Cutkosky, M. R., 1996, ''Practical Force-Motion Models for Sliding Manipulation,'' Int. J. Robot. Res., **15**(6), pp. 557–572.
[6] Johnson, K. L., 1985, *Contact Mechanics*, Cambridge University Press, Cambridge, UK.
[7] Kluger, M. A., and Fussner, D. R., 1997, ''An Overview of Current CVT Mechanisms, Forces and Efficiencies,'' SAE Technical Paper Series 970688.
[8] Singh, T., and Nair, S. S., 1992, ''A Mathematical Review and Comparison of Continuously Variable Transmissions,'' SAE Technical Paper Series 922107.
[9] Kim, J., Yeom, H. J., and Park, F. C., 1999, ''MOSTS: A Mobile Robot with a Spherical Continuously Variable Transmission,'' *IEEE/RSJ International Conference on Intelligent Robots and Systems*, pp. 1751–1756.
[10] Sordalen, J. J., Nakamura, Y., and Chung, W. J., 1994, ''Design of a Nonholonomic Manipulator,'' *IEEE International Conference on Robotics and Automation*, pp. 8–13.